Published Journal Article available at: http://dx.doi.org/10.1016/j.compstruct.2016.12.012

Acoustic emission and damage mode correlation in textile reinforced PPS composites

Valter Carvelli [a, *], Alessandro D'Ettorre [a], Stepan V. Lomov [b]

[a] Department A.B.C., Politecnico di Milano, Piazza Leonardo da Vinci 32, 20133 Milano, Italy
[b] Department of Materials Engineering, K.U. Leuven, Kasteelpark Arenberg 44, B-3001 Leuven, Belgium

The paper applies the cluster analysis methodology to thermoplastic Polyphenylene sulphide (PPS) carbon woven com-posites. The experimental quasi-static tensile tests were assisted by: a digital camera for digital image correlation (DIC) evaluation of the full field strain; a digital camera for local damage observation; acoustic emission (AE) sensors for mea-surement of the acoustic emission features during loading. The experimental data and the subsequent cluster analyses of the AE events show a similar distribution of the AE clusters for the considered thermoplastic carbon composites and other thermoset woven composites described in the literature. The boundaries of those clusters are different for some extent, while a typical damage mechanism, namely transverse cracks inside the yarns, was clearly correlated to the first cluster with lower amplitude and lower frequency acoustic events.

Keywords: Thermoplastic, Textile composites, Acoustic emission, Cluster analysis, Damage

1. Introduction

Acoustic emission (AE) registration with subsequent analysis of the AE event parameters is a recognised and widely used method for damage monitoring during loading of fibre reinforced composites, which provides information of damage processes in the specimen without stopping the test, at a good time resolution, also identifying the spatial origin of the events. Quasi-static tension test is probably the most common type of loading for which AE registration is routinely used.

AE is useful for identification of damage thresholds: load (or strain) levels which manifest different stages of damage development (Fig. 1). The first damage in textile composites typically appears in the form of transverse (to the loading direction) cracks inside the yarns or on the yarn boundaries (short designation: *t*). Cracks are developed by coalescence of initial micro-debondings on the fibre-matrix interface. Upon further load increase, the transverse cracks propagate along the yarn length. They also increase in numbers until a certain critical number is reached (saturation). Transverse cracks in resin rich pockets (*tm*) are usually cracks that originated inside yarns but then propagated into these areas. When the transverse cracks are well developed, they cause appearance of the local delaminations (*l*), triggered by shear stresses resulting from interaction of the transverse cracks with the longitudinal reinforcement. The longitudinal yarns are subject to Poisson contraction under tension; this deformation is constraint by the presence of the transverse yarns, which leads to development of tensile transverse stresses in the longitudinal yarns. When the transverse strength of the longitudinal yarns is exceeded by these stresses, they can start splitting (*sp*). The local delaminations progress, leading to larger inter-ply delaminations (*L*). The onset and propagation of delaminations between plies is dependent on the interlaminar fracture toughness of the composite. In the final stage, massive breakage of fibres in longitudinal yarns begins (*f*). The strain at which this happens in textile composites is typically below the ultimate strain of fibres. This reduction is caused by the fibre crimp and developed delaminations, which prohibit efficient stress transfer inside fibre bundles.

Fig. 1 presents this sequence of damage events. It suggests presence of two thresholds of the applied load. The first, designated as ε_1, corresponds to the onset of the transverse cracking (*t*-cracks), which may not at this stage span the whole width of the specimen, being limited by the yarn crimp and/or presence of stitching in the textile reinforcement structure. The second, designated as ε_2, corresponds to, on one hand, the onset of local delaminations (*l*-cracks) and, on the other hand, to the formation of "strong" transverse cracks, which span the width of the specimen.

The damage thresholds can be identified using acoustic emission (AE) registration during the tensile loading. In [1–3], it was proposed to use a curve of cumulative energy (*E*) of the AE events for identification of the damage thresholds. The reader is referred also to [3] for details of the procedure of the damage thresholds identification using logarithmic and linear scales for the $E(\varepsilon)$ curve, as adopted for the material studied in the present paper (see Section 4.2). This methodology was also applied in [4] for damage investigation in 5H satin carbon/PPS composites.

In the last five years, studies for the identification of the damage modes in fibre reinforced composites using cluster analysis added frequency and other descriptors of the AE events (e.g. [5–8]). The role of the frequency descriptors is not, however, generally accepted. For example, in [9] the cluster analysis has led to a conclusion that

Article history:
Received 24 October 2016
Received in revised form 28 November 2016
Accepted 5 December 2016
Available online xxx

* Corresponding author.
Email address: valter.carvelli@polimi.it (V. Carvelli)

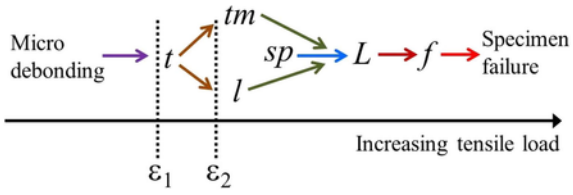

Fig. 1. A typical sequence of damage development in textile composites under tension loading.

for flax reinforced thermoplastic composites the amplitude is the discriminating parameter for damage modes; frequency is not included in the set of descriptors. In [10], similar conclusion is drawn for the case of glass/epoxy composites in an open hole tensile test.

In [11–13], some of the present authors applied the approach of the damage mode identification based on the cluster analysis of AE events parameters to textile composites with thermoset matrices, which allowed physically based identification of the damage thresholds. These papers advance the methodology of the damage type identification, previously adopted by the authors (see e.g. [1–3,14]), which was based only on the acoustic energy thresholds, to the unsupervised cluster analysis, accounting also for the signal frequency. The pair of AE parameters (amplitude + a frequency parameter) was found to be the most important to discriminate the damage modes in tension loading of glass/epoxy and carbon/epoxy 2D and 3D woven composites. The cluster analysis of the AE events (presented briefly in Section 3) identifies typically three clusters of the events in the multi-parametric event space. The most important of the event parameters are the AE signal amplitude (expressed in dB and strongly correlated with the logarithm of the AE event energy) and one or another frequency-related parameters (peak frequency or frequency centroid). As shown in [11–13], in carbon/epoxy woven laminates the three clusters contain events originated from transverse matrix cracks (events with low frequency and low amplitude), local delaminations (low frequency and high amplitude) and fibre breakage (high frequency). The load values, corresponding to the onset of the AE events in the first and the second cluster correspond to the damage threshold values ε_1 and ε_2, respectively.

The present paper for the first time, in the Authors' knowledge, applies the cluster analysis methodology to thermoplastic (PPS) carbon woven composites. The research questions of the paper are: (1) is clustering of AE events in carbon woven composites with a brittle thermoplastic matrix the same as in similar composites with thermosetting matrix? (2) is there a difference in the cluster boundaries between these two types of composites? (3) can AE events in different clusters be identified with different damage modes?

The experimental investigation and the subsequent cluster analyses show a similar distribution of the AE cluster for the considered thermoplastic carbon composites and other thermoset woven composites described in the literature. The boundaries of those clusters are different for some extent, while a typical damage mechanism, namely transverse cracks inside the yarns, was clearly correlated to the first cluster with lower amplitude and lower frequency acoustic events.

2. Composite material and experimental procedure

Composite panels (41 × 41 cm) were fabricated using Polyphenylene sulphide (PPS) matrix (Ticona Fortron® 0205 [15]) and a five-harness satin weave carbon textile as reinforcement, whose main features are in Table 1a. The composite ($[(0, 90)]_3$) is similar to that adopted for the investigation detailed in [16], with the difference in fibre volume fraction, which is higher in the material studied in the present paper.

Table 1
Main characteristics (a) of the fabric reinforcement and (b) of the composite panels.

(a)	
Carbon Fibres	Torayca T300 J
Yarns	3 K
Yarn linear density [tex]	198
Fabric density [g/m^2]	285
Ends count [yarns/cm]	7
Pick count [yarns/cm]	7
(b)	
Number of plies	6
Fibre volume fraction [%]	57.6 ± 1.8
Thickness [mm]	1.65 ± 0.09

Measurements of the thickness and fibre volume fraction of the panels are listed in Table 1b.

Specimens for tensile test were extracted having the dimensions, according to standard ASTM D3039: total length 260 mm, gage length 160 mm, width 25 mm.

Tensile tests were performed using an Instron 4505 with a crosshead speed of 1 mm/min applying the load in the warp direction (considering the reinforcement balanced).

The experimental tests were divided in three sets.

Specimens of the first set were loaded up to failure to measure the main mechanical properties (elastic modulus and strength).

Specimens of the second and third set were equipped with two AE sensors (Digital Wave B-1025), 15 mm from each tab, to record the acoustic emission up to the 70% of the average ultimate tensile strength (from the first set of tests). This load level was set to avoid damage of the acoustic equipment. Details of the software and sensors for the AE recording are in Table 2. The parameters of the AE signals (energy, amplitude, frequency, etc.) were calculated using the standard functionalities of the adopted software (see Table 2).

For the second set of tests, AE were recorded in the complete zone between the two sensors (distance of 130 mm, see Fig. 2), while for the third set of specimens AE localized in the centre for a length of 5 mm were distinguished. This was used for the correlation of the acoustic emissions and the damage mode. In the same central zone, crack development was observed taking images (frequency 2 Hz) of the thickness of the specimens by the first CCD camera (size 1392 × 1040, 1.45 MP) (Fig. 2).

Before tests with AE recording, pencil tests were carried out on each specimen. Three 0.7 mm 2H pencil leads were broken in the centre of the specimen while registering AE. This allowed to check the accuracy of the AE location registered by the sensors and the actual location of events.

During loading of all specimens, images were acquired (frequency 2 Hz) using a LIMESS system, consisting of the second CCD camera (same features of the first one) (Fig. 2), and software for calibration

Table 2
Features of the software and sensors for the acoustic emission recording.

Software	Vallen AMSY-5
Amplifiers	Vallen AEP4
Amplification [dB]	34
Discrimination time [ms]	0.4
Rearm time [ms]	3.2
Range [MHz]	0.0025÷1.6
Sample rate [MHz]	5
Sensors	Vallen VS375S-M
Sensor diameter [mm]	20
Threshold [dB]	40

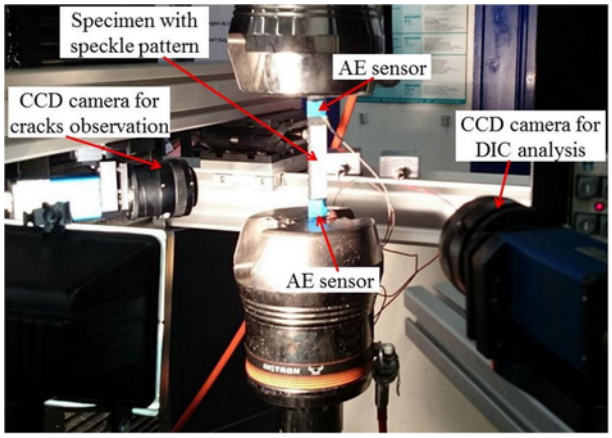

Fig. 2. Test set-up.

and recording. The images post-processing allowed the measurement of the full field strain on the external surface of the specimen by the digital image correlation technique (DIC) adopting the vic-2D software [17]. For this purpose, one side surface of the specimen, for a length of about 80 mm in the centre, was speckled with white and black acrylic paints (Fig. 2). Some parameters adopted for the DIC analyses were: subset size 40, step size 3 and filter size 15.

3. Theoretical background of the AE clustering

The AE clustering technique adopted is detailed in [11] and [13]. Here a brief description is summarized for symbols and concepts.

The acoustic emission features considered here were nine: peak amplitude (A); duration (D); energy (E), i.e. the area under the voltage-time envelope; counts (CNTS), i.e. the comparator output pulses corresponding to the threshold crossings; rise time (R), i.e. the time interval from the first threshold crossing to the maximum amplitude; frequency centroid (FCOG); peak frequency (FMAX); weighted frequency value (WF); RA value, i.e. rise time divided by amplitude.

The statistically representative features for further analysis were selected considering two parameters:

- Laplacian Score (LS): it ranges between 0 and 1, a larger score indicates a higher cluster ability of the investigated feature;
- Correlation Coefficient (CC): it ranges from 0 to 1 and shows how features are correlated and dependent one with the other.

The features with the best LS and CC were used for the clusters generation by the principal component analysis (PCA) and the k-means++ algorithm [11].

PCA is an orthogonal linear transformation of multidimensional AE data into lower dimension set (a new coordinates system) of uncorrelated features that are the principal components.

The k-means++ is a modified release of the k-means algorithm, based on an iterative algorithm in which a predefined number 'k' of centroids is spread throughout the data and the data samples are allocated to the closest centroid.

The proper number of clusters was evaluated considering [11]:

- Silhouette coefficient (SC): it has a value between 0 and 1, the score is higher when clusters are dense and well separated;
- Davies-Bouldin index (DB): based on a ratio of within-cluster and between-cluster distances and it relates to the cluster centroids.

The best cluster quality has the lower DB index and the higher SC coefficient.

4. Results and discussion

The available specimens were divided in three sets for different measurements and observations. Two specimens were loaded up failure to measure the tensile elastic modulus and strength. Eight specimens were loaded up the 70% of the tensile strength for recording the AE and selecting the main AE features for clusters construction. Three specimens of the latter set were adopted for crack monitoring in a small portion of the thickness and for the correlation of the acoustic emissions and the observed cracks.

For each set, the number of specimens could not be statistically significant but, however, they provide a clear understanding on the cluster analysis and cracks correlation.

4.1. Tensile mechanical properties

The quasi-static tensile tests up to failure were necessary for the tensile static strength, which is needed, in turn, for setting the maximum stress level for further tests with AE recording.

The recorded stress-strain curves are depicted in Fig. 3 and show good reproducibility of the results. The strain component was calculated as average in the speckle portion by DIC. In Fig. 3, two curves are for loading up to complete failure, while the others are for specimens equipped with AE sensors loaded up to almost 70% of the average strength. Those curves provide the main average tensile mechanical properties of the thermoplastic composite collected in Table 3. The measured modulus, according to standard ASTM D3039, of 63 GPa, after scaling with fibre volume fraction (57% for the material studied here) is in agreement with the ones reported for the same re-

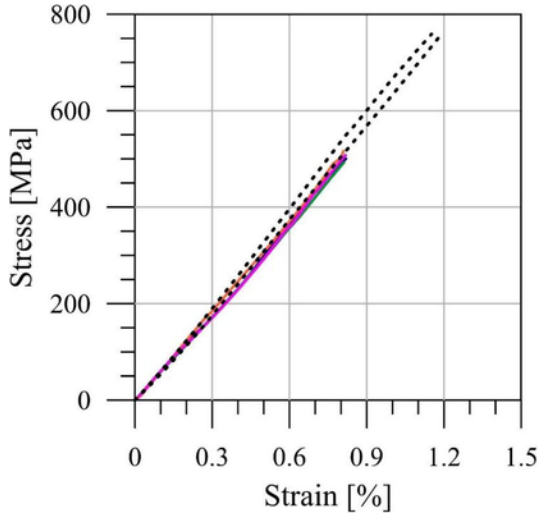

Fig. 3. Stress vs. strain curves: dashed line up to failure; continuous line up to 70% of the strength.

Table 3
Longitudinal quasi-static mechanical properties of the composite. Ultimate properties (σ_u, ε_u), average of two measurements; initial elastic modulus (E), average and standard deviation of seven measurements.

E [GPa]	63.2 ± 1.9
σ_u [MPa]	764.5
ε_u [%]	1.19

inforcement/matrix system in [4] (57 ± 1 GPa for FVF = 50 ± 3%) and in [16] (58.5 ± 1.2 GPa for FVF = 53 ± 0.5%).

The stress-strain curves are almost linear. However, considering the tangent modulus, the non-linearity is evident. Table 4 shows the average tangent modulus determined from two stress-strain curves as a function of the applied strain. The modulus increases by 12% with the increase of the strain from 0.05% to 0.8%; similar measurement was recorded in [1,14] for carbon multiaxial multiply stitched composites and carbon 3D braided carbon/epoxy composites, respectively. This is attributed to two factors: the inherent stiffening of carbon fibres under tensile loading ([18,19]); the weave structure of carbon fabrics changing the local fibre orientation in the composite due to their straightening under increasing tensile load.

The observed decrease of the tangent modulus highlights the "softening" behaviour of the material at the higher strain levels, above 0.8% (see Table 4). It can be explained by a dominant effect of matrix cracking on the fibre stiffening, leading to failure. This is the main reason the specimens equipped with AE sensors were loaded up to 70% of the average strength, meaning strain level of about 0.8% (see Fig. 3).

4.2. AE events and clusters analysis

The AE equipment records acoustic events and registers the energy and other features of the individual events.

Energy of the AE events (Fig. 4a) and their locations in between the two sensors (Fig. 4b) are shown for a representative specimen, together with stress-strain relationship. For all specimens, most of the AE events had energy lower than 10^3 and few events had relatively high energy more than 10^6. Similar distribution was observed in [5] for unidirectional carbon/epoxy and for E-glass plain weave/epoxy in [11], while for a single-ply non-crimp 3D orthogonal E-glass woven/epoxy the large part of the events had energy in the range 10^5–10^6 [11].

A processing of the AE energy generates the curve of cumulative energy. The cumulative energy curves of five specimens, in the second set, show a good repeatability of the tests, as detailed in Fig. 5a. From the cumulative energy curve, the strain levels for damage initiation and development can be detected as abrupt slope variations, i.e. "knees". In particular, three characteristic strain levels are selected according to [2], namely: ε_{min}, ε_1 and ε_2. The average of those strain levels are detailed in Fig. 5b. The recorded values of the strain thresholds reveal an earlier initiation and development of the damage compared to epoxy matrix reinforced carbon composites. The 3D rotary braided carbon/epoxy composite investigated in [14] had the first threshold for an average strain of 0.12%, while the second was for 0.35%. Similarly, the three-axial braided carbon/epoxy composite detailed in [2] had as first and second strain levels 0.3% and 0.5%, respectively. The early damage events in the PPS composite compared to epoxy ones could be consequence of the thermal residual stresses accumulated during the manufacturing, as observed in [4] and based on the literature on thermo-plastic composites (see e.g. [20,21]). The release of the residual stresses leads to an initial steep increase of the cumulative energy (see Fig. 5a).

The measured values of the damage thresholds of $\varepsilon_1 = 0.10 \pm 0.03\%$ and $\varepsilon_2 = 0.15 \pm 0.05\%$ are significantly lower than the ones measured in [4] for the similar material as $\varepsilon_1 = 0.3 \div 0.35\%$ and $\varepsilon_2 = 0.4 \div 0.45\%$. The reason for this shift of the damage thresholds can be found in the different fibre volume fraction, which is 57% for the present material and 50% for the one in [4]. This difference of the overall fibre volume fraction (FVF) is translated in large difference in fibre volume fraction inside the yarns (called FVF_y below for brevity). The value of FVF_y given in [22] is 70%. With the increase of the overall fibre volume fraction from 50% to 57%, assuming the same volume fraction of the yarns, FVF_y will increase to 80%. This high fibre volume fraction is impossible to achieve without tightly compacted fibre configurations, which lead to extreme stress concentrations between the fibres, early damage initiation and facilitate also formation of a continuous transverse crack from micro-level fibre-matrix debonding.

Table 4
Average (two tests) longitudinal tangent modulus as function of the applied strain.

Strain [%]	0.05	0.3	0.5	0.8	0.9	1.1
Tangent modulus [GPa]	60.73	64.87	65.13	68.54	67.83	63.51

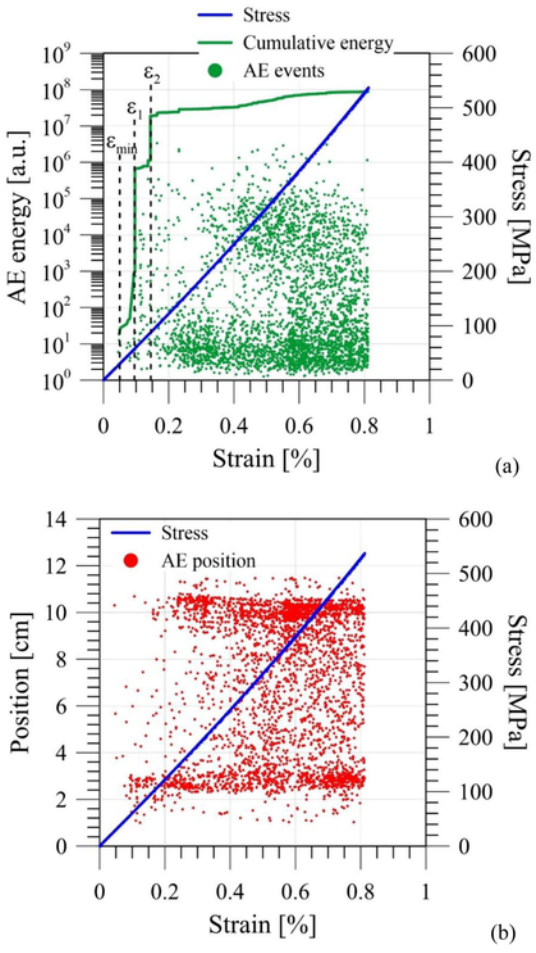

Fig. 4. Representative (a) AE events, AE cumulative energy and stress vs. strain (b) position of the AE events and stress vs. strain.

The proper AE features for the cluster analysis were selected considering the Laplacian score and the Correlation coefficient [11]. The selection procedure allowed to distinguish the irrelevant and redundant AE features and to choice those to be used in the cluster analysis. Four AE parameters, out of nine, were chosen, namely: peak amplitude (A), peak frequency (FMAX), frequency of centroid (FCOG) and RA value. The same parameters were selected by the same algorithm for other glass and carbon textile composites in [11] and [13].

Principal component analysis (PCA) provided the variance percentage and cumulative variance of each principal AE component. A representative illustration is detailed in Fig. 6a. The first and the

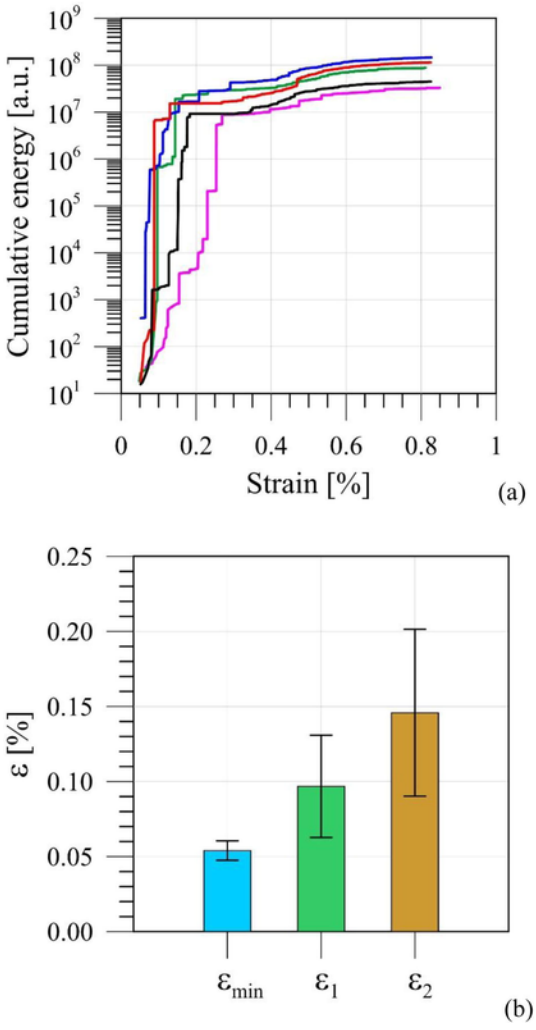

Fig. 5. (a) AE cumulative energy vs strain of all specimens of the second set and (b) average strain thresholds (bars represents the standard deviation of five tests).

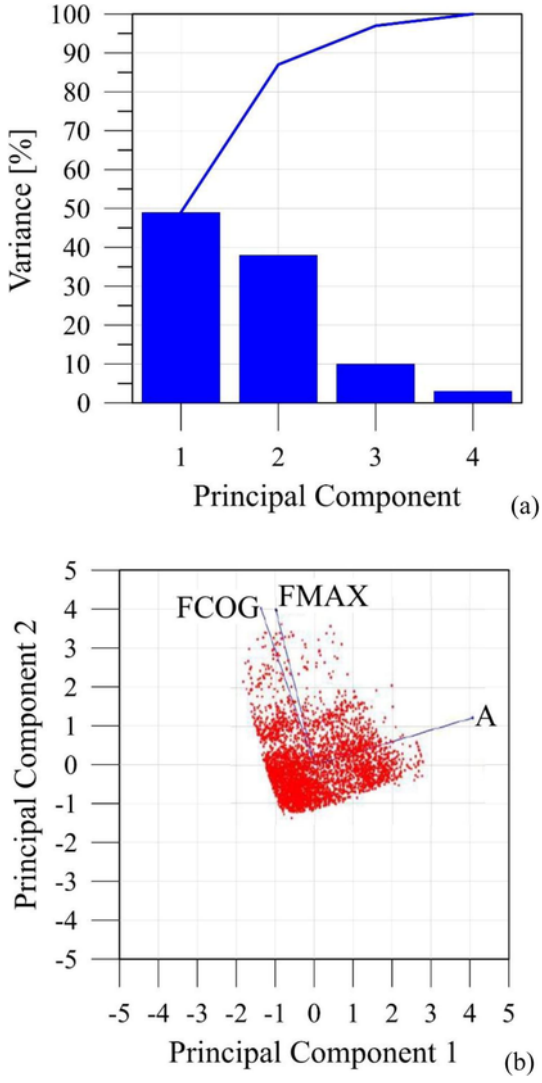

Fig. 6. Representative Principal Components Analysis: (a) Variance (bars) and cumulative variance (line) of each principal component; (b) component coefficients of AE parameters for the first two principal components.

second principal components generates more than 80% of the total variance, meaning that the two components can visualize the AE data. The coefficients of the two principal components indicate that the largest is that of A, while those related to FMAX and FCOG are quite similar (see Fig. 6b). For the clusters representation, A and FCOG were selected for the better separation of the clusters points in the space of these two parameters (see Fig. 8).

The number of clusters for the analysis of a complete set of AE was supposed considering the Silhouette coefficient (SC) and the Davies-Bouldin index (DB). The typical comparison in Fig. 7 shows that the best choice is three clusters, as obtained for other thermoset reinforced carbon textile composites in [13]. The representation of the AE events, in the A-FCOG coordinates, highlighted a good separation (Fig. 8), as mentioned, of the three clusters (CL1, CL2, CL3). The separation of the clusters, in term of A and FCOG are summarized in Table 5. The present carbon textile reinforced thermoplastic resin (PPS) had similar value for the A bound to other carbon textiles reinforced thermoset resin (epoxy), while the frequency is almost double (Table 5). The variation of frequency bound becomes even higher (about five times) comparing with glass textile reinforced epoxy materials investigated in [11]. It must be mentioned that the comparison in Table 5 is supposed considering either the peak frequency (FMAX) or the frequency centroid (FCOG), according to the better cluster subdivision for the different materials. Data listed in Table 5 from [13] were measured with the same AE events recording system and the same two sensors placed at the same distance on specimens of similar dimensions, as in the present investigation.

Several investigations in the literature deduced a correlation of some ranges of AE features with different damage mechanisms (for glass reinforced, e.g., [12], [23], [24], and carbon reinforced, e.g., [5], [25] composites). Low-amplitude and low-frequency AE events in CL1 were connected to matrix cracking; AE events in CL2 can be attributed to fibre-matrix debonding; high-peak frequency AE events (CL3) were related to delamination and to fibres breakage. The bounds of each cluster depend on the peculiarities of the considered composite materials (see e.g., [13,5]). The relatively high frequency delimiting the clusters for the present thermoplastic carbon reinforced material, as compared to other thermoset ones, could be supposed related to a reduced sequences of delamination, and fibres breakage are mainly responsible of the AE in cluster CL3. This hypothesis is not supported by direct observation and needs further in depth investigations. Direct observations and correlations of damage mechanisms

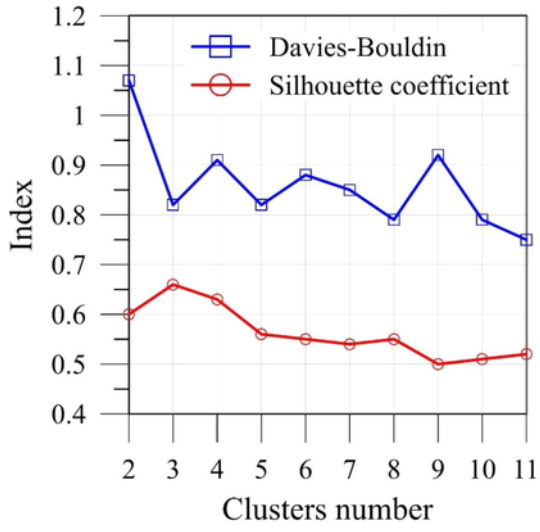

Fig. 7. Representative diagram of the Silhouette coefficient and Davies–Bouldin index for selection of the number of clusters considering the complete set of AE.

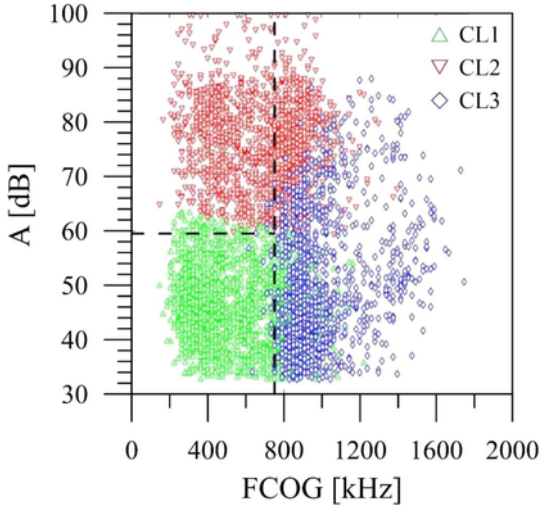

Fig. 8. Representative clusters in the plane A-FCOG for the complete set of AE.

Table 5
Cluster bounds for the present carbon textile reinforced PPS (CF/PPS), a 3D and a 2D carbon textile reinforced epoxy.[13]

Cluster	CF/PPS		3D carbon/epoxy [13]		2D carbon/epoxy [13]	
	A [dB]	FCOG [kHz]	A [dB]	FCOG [kHz]	A [dB]	FMAX [kHz]
CL1	<60	<800	<60	<400	<70	<300
CL2	>60	<800	>60	<400	>70	<300
CL3	30–90	>800	30–90	>400	30–90	>300

with clusters of AE events was not extensively investigated and reported in the literature. This is supposed to be covered in the next section, where the connection of AE events in CL1 and a damage mechanism is detailed.

4.3. Correlation of damage mechanism and cluster of AE events

The damage mechanisms in a small central portion of three specimens were observed during tensile loading and, simultaneously, AE were recorded and selected according to the localization in the considered zone. The continuous observation by a CCD camera of the thickness surface allowed to detect the cracks initiation and development and to link pictures to the average strain level, calculated by DIC post processing, during the full loading history. The AE events recorded between the two sensors were adopted for two clusters analyses: the first considering the full set of events; the second using the AE localized in the portion of the specimen, where the damage was detected on the thickness side. The two cluster analyses were considered to assess the accuracy and reproducibility of the information with two different sets of events and to distinguish the cluster related to a specific damage mechanism. Considering the AE events located in the central portion of 5 mm under observation, the Silhouette coefficient (SC) and the Davies-Bouldin index (DB) suggests the selection of three clusters (see typical comparison in Fig. 9). This lead to a clear distinction of the clusters by the amplitude and the peak frequency (Fig. 10a). It is consistent with the analysis of the full set of AE events, whose clusters have a better representation in the A-FCOG coordinates (Fig. 10b). The comparison of the two representations is reasonable having similar coefficients of the two principal components related to FMAX and FCOG (see Fig. 6b).

Pictures in Fig. 11 show the cracks observed at different strain level for a representative specimens. Red circles highlight intra-yarns matrix cracks generated by the manufacturing process ($\varepsilon = 0\%$) or existing cracks from the previous load levels. Those pictures allowed the counting of the new cracks (white circles) at each strain level and their accumulation is represented in Fig. 12.

The appearance of a new crack generates an acoustic event localized in the zone of observation. The synchronization of the different signals allowed to link the AE in each cluster to the strain level, as detailed in Fig. 13a, and, in particular, to have the number of the AE at each strain level in the considered zone. The latter is supposed to be generated by the same number of damage events. Focussing the attention on the cumulative number of AE belonging to

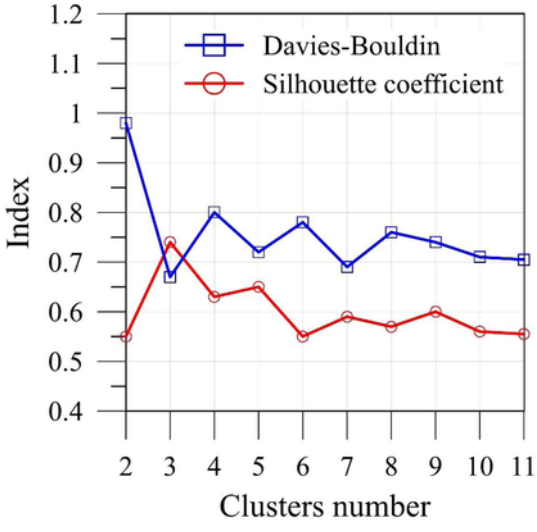

Fig. 9. Silhouette coefficient and Davies–Bouldin index for selection of the number of clusters considering the set of AE in the zone for cracks observation. Same specimen as for Fig. 6.

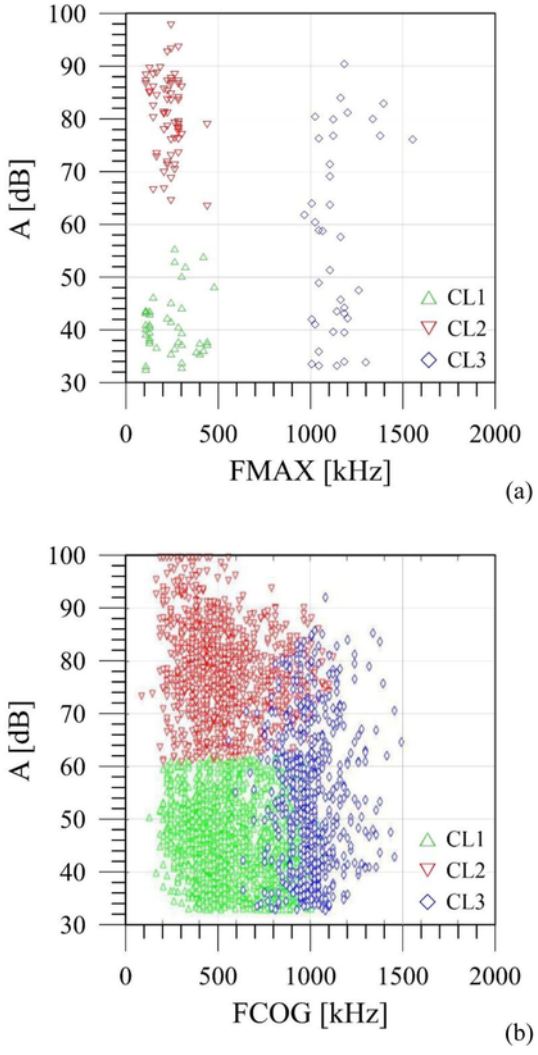

Fig. 10. Clusters including: (a) AE events in the zone for damage observation; (b) full set of AE.

CL1, represented in Fig. 13b, events were recorded for strain higher than 0.1% and intra-yarn matrix cracks appeared after the same strain level (see Fig. 12). Moreover, the number of AE events of CL1 and the number of cracks are quite similar. Therefore, comparing the number of new cracks and the AE events in CL1, at each strain level, a perfect match was observed as shown in Fig. 14, at least up to a strain of 0.6%. For higher strain, the number of AE in CL1 was higher than the number of observed cracks. This means that similar cracks did not occur on the observed surface of the thickness, but inside or on the opposite side of the same portion. However, the comparison in Fig. 14 gives a clear connection of the AE in the CL1 and the damage mode, namely intra-yarn matrix crack.

The repeatability of the procedure and of the correlation was demonstrated by other specimens of the same material, as detailed in Fig. 15. The discrepancy in Fig. 15b is motivated, as mentioned, considering the cracks generated in positions outside the observed surface.

The correlation, above presented, was suppose assuming the AE in the CL1, being this considered in the literature related to matrix cracking. This is confirmed in the present context. For the specimen adopted for Fig. 13, the AE events belonging to CL2 were: 2 in the strain range 0.2–0.3%; 2 in the strain range 0.3–0.4%; 1 in the range 0.8–0.83%. This is not compatible with the crack counting, being the number of cracks observed in the same strain ranges: 3, 4 and 2, respectively. Same argument is valid for AE in CL3, e.g., for strain below 0.3%, the number of AE is lower than the nine cracks observed. Therefore, assuming that each crack is associated to an AE event, a higher amount of cracks than AE events cannot be justified. This allowed to claim that AE events in CL2 and CL3 are not associated to intra-yarn matrix cracking.

5. Conclusions

The main aim of the investigation was the application, for the first time in the Authors' knowledge, of the AE cluster analysis methodology to thermoplastic (PPS) carbon woven composites.

The research got the following answers to the three research questions, namely: (1) is clustering of AE events in carbon woven composites with a brittle thermoplastic matrix the same as in the similar composites with thermosetting matrix? (2) is there a difference in the cluster boundaries between these two types of composites? (3) can AE events in different clusters be identified with different damage modes?

(1) The adopted clusters analysis methodology, for the complete set and local set of AE events, suggested three as the optimal cluster number for the considered thermoplastic reinforced carbon woven composite. The same number of distinct and well-separated clusters was the best choice for previously studied thermoset reinforced carbon textile composites.

(2) The separation of the clusters for the present carbon textile reinforced thermoplastic resin (PPS) had similar value for the amplitude (dB) boundary to other carbon textiles reinforced thermoset resin, while the frequency centroid value is almost double. The variation of frequency bound becomes even higher (about five times) comparing with glass textile reinforced epoxy materials. This reduces the credibility of the interpretation, in previous works, which linked the frequency-related cluster boundary to the properties of the fibres. Apparently this boundary is defined by a combination fibres/matrix.

(3) The cracks development observed in a small central portion was connected to the AE events located in the same zone of the specimen. The number of new intra-yarn matrix cracks generates at each strain level was compared to the number of acoustic event localized in the zone of observation. A good agreement was identified between the number of AE events of CL1 (low amplitude and low frequency) and the number of observed cracks. Therefore, a clear correlation of the AE events in CL1 and the intra-yarn matrix cracks was established.

The latter understanding cannot be considered exhaustive and must be corroborated by other direct correlations using different thermoplastic reinforced carbon woven composites.

However, based on the present achievements, future investigations are supposed to confirm the present results and to have the same direct correlation of the AE events belonging to CL2 and CL3 with other damage mechanisms (fibre-matrix debonding, delamination and fibre breakage), as supposed in the literature.

Acknowledgement

The research visit of A. D'Ettorre to KU Leuven was partially funded by Erasmus program of EU and a scholarship of Politecnico di Milano.

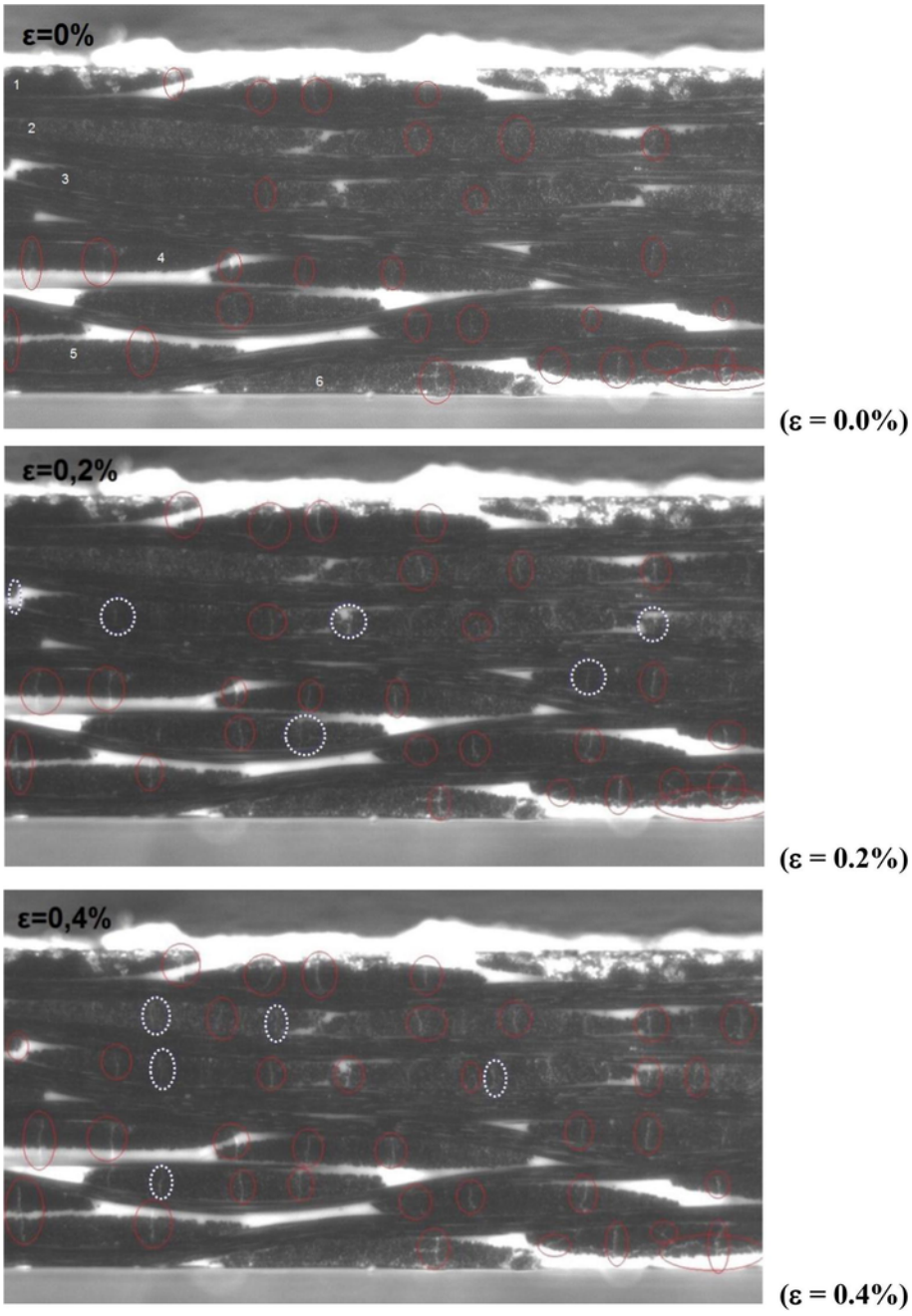

Fig. 11. Counting of cracks in the observed zone of the thickness for different strain levels. Red ellipses show existing cracks. White dashed ellipses mark new cracks. (For interpretation of the references to colour in this figure legend, the reader is referred to the web version of this article.)

Dr. Li Li is gratefully acknowledged for the script implementing the cluster analysis technique.

TenCate (The Netherlands) is acknowledged for manufacturing and supplying (in the framework of EU FP7 project M-RECT) the composite material plates adopted in this investigation.

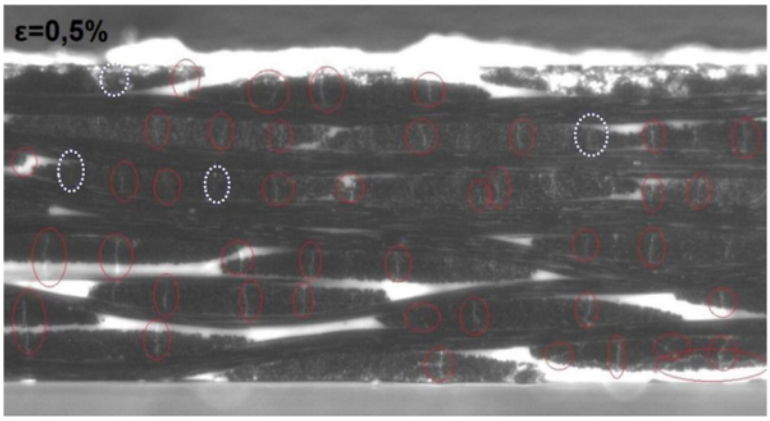

(ε = 0.5%)

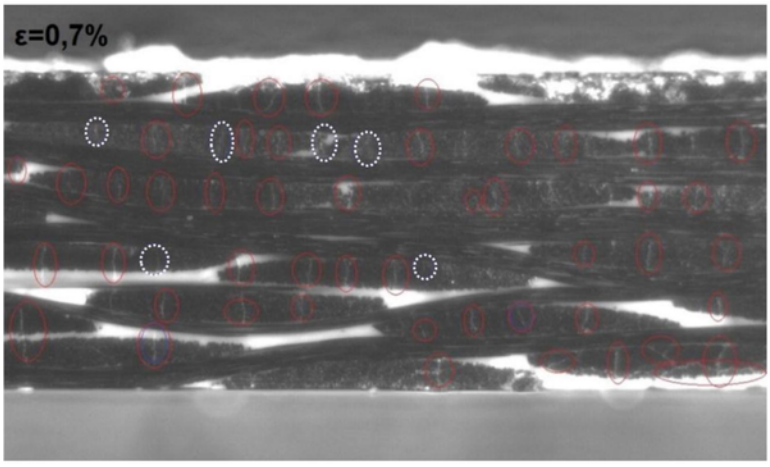

(ε = 0.7%)

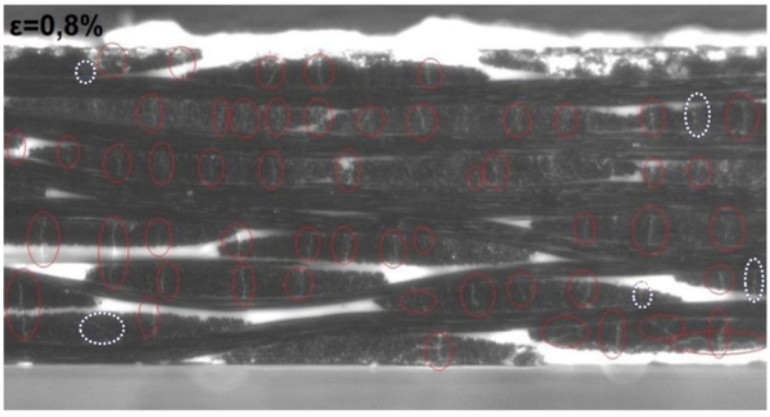

(ε = 0.8%)

Fig. 11. (*Continued*)

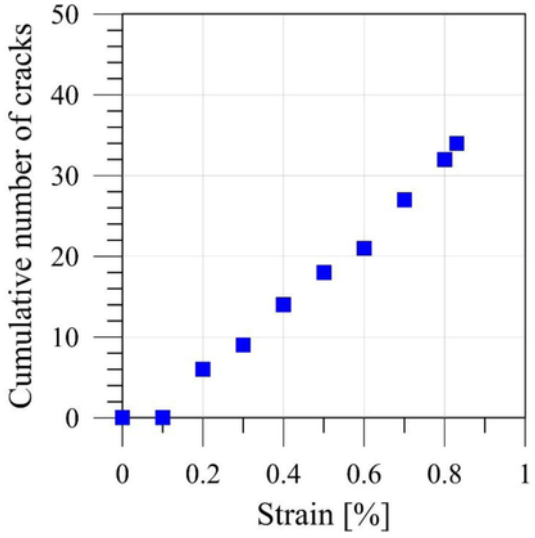

Fig. 12. Cumulative number of cracks in the observed zone vs. strain.

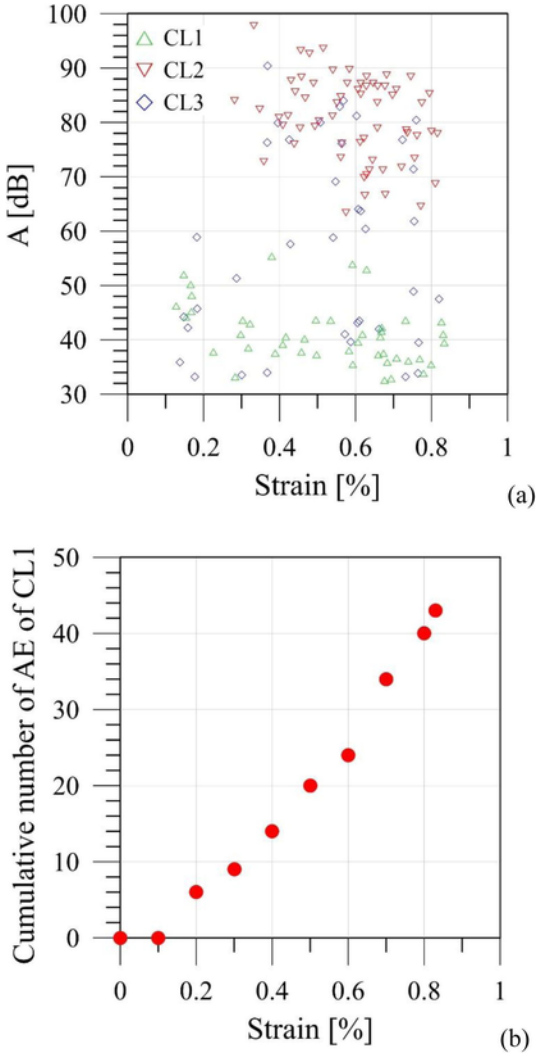

Fig. 13. (a) Amplitude of the AE in the zone for cracks observation vs. strain; (b) cumulative number of AE in the Cluster 1 vs. strain.

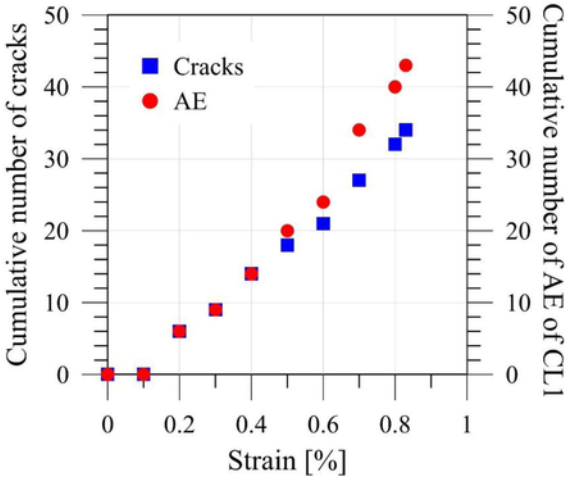

Fig. 14. Comparison of the cumulative number of cracks and cumulative number of AE in the Cluster 1 vs. strain.

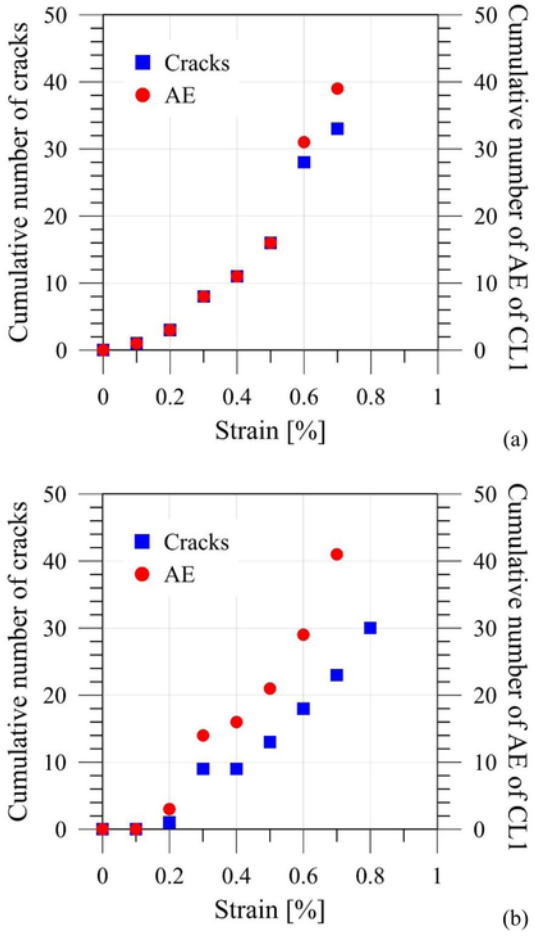

Fig. 15. Comparison of the cumulative number of cracks and cumulative number of AE in the Cluster 1 vs. strain for two other specimens.

References

[1] T. Truong Chi, M. Vettori, S.V. Lomov, I. Verpoest, Carbon composites based on multiaxial multiply stitched preforms. Part 4: mechanical properties of composites and damage observation, Composites A 36 (2005) 1207–1221, http://dx.doi.org/10.1016/j.compositesa.2005.02.004.

[2] S.V. Lomov, D.S. Ivanov, T.C. Truong, I. Verpoest, F. Baudry, K. Vanden Bosche, H. Xie, Experimental methodology of study of damage initiation and development in textile composites in uniaxial tensile test, Compos Sci Technol 68 (2008) 2340–2349, http://dx.doi.org/10.1016/j.compscitech.2007.07.005.

[3] S.V. Lomov, A. Bogdanovich, D. Ivanov, D. Mungalov, M. Karahan, I. Verpoest, A comparative study of tensile properties of non-crimp 3D orthogonal weave and multi-layer plain weave E-glass composites. Part 1: materials, methods and principal results, Composites A 40 (8) (2009) 1134–1143, http://dx.doi.org/10.1016/j.compositesa.2009.03.012.

[4] S. Daggumati, I. De Baere, W. Van Paepegem, J. Degrieck, S..Lomov. Xu, I. Verpoest, Local damage in a 5-harness satin weave composite under static tension: part I – experimental analysis, Compos Sci Technol 70 (2010) 1926–1933, http://dx.doi.org/10.1016/j.compscitech.2010.07.003.

[5] R. Gutkin, C.J. Green, A. Vangrattanachai, S.T. Pinho, P. Robinson, P.T. Curtis, On acoustic emission for failure investigation in CFRP: pattern recognition and peak frequency analyses, Mech Syst Signal Process 25 (2011) 1393–1407, http://dx.doi.org/10.1016/j.ymssp.2010.11.014.

[6] M. Sause, A. Gribov, A. Unwin, S. Horn, Pattern recognition approach to identify natural clusters of acoustic emission signals, Pattern Recogn Lett 33 (2012) 17–23, http://dx.doi.org/10.1016/j.patrec.2011.09.018.

[7] C. Baker, G. Morscher, V. Pujar, J. Lemanski, Transverse cracking in carbon fiber reinforced polymer composites: modal acoustic emission and peak frequency analysis, Compos Sci Technol 116 (2015) 26–32, http://dx.doi.org/10.1016/j.compscitech.2015.05.005.

[8] E. Maillet, C. Baker, G. Morscher, V. Pujar, J. Lemanski, Feasibility and limitations of damage identification in composite materials using acoustic emission, Composites A 75 (2015) 77–83, http://dx.doi.org/10.1016/j.compositesa.2015.05.003.

[9] A. Monti, A. El Mahi, Z. Jendli, L. Guillaumat, Mechanical behaviour and damage mechanisms analysis of a flax-fibre reinforced composite by acoustic emission, Composites A 90 (2016) 100–110, http://dx.doi.org/10.1016/j.compositesa.2016.07.002.

[10] J. Jefferson Andrew, V. Arumugam, D. Bull, H. Dhakal, Residual strength and damage characterization of repaired glass/epoxy composite laminates using A.E. and D.I.C, Compos Struct 152 (2016) 124–139, http://dx.doi.org/10.1016/j.compstruct.2016.05.005.

[11] L. Li, S.V. Lomov, X. Yan, V. Carvelli, Cluster analysis of acoustic emission signals for 2D and 3D woven glass/epoxy composites, Compos Struct 116 (2014) 286–299, http://dx.doi.org/10.1016/j.compstruct.2014.05.023.

[12] L. Li, S.V. Lomov, X. Yan, Correlation of acoustic emission with optically observed damage in a glass/epoxy woven laminate under tensile loading, Compos Struct 123 (2015) 45–53, http://dx.doi.org/10.1016/j.compstruct.2014.12.029.

[13] L. Li, Y. Swolfs, I. Straumit, X. Yan, S.V. Lomov, Cluster analysis of acoustic emission signals for 2D and 3D woven carbon fiber/epoxy composites, J Compos Mater 50 (2016) 1921–1935, http://dx.doi.org/10.1177/0021998315597742.

[14] V. Carvelli, J. Pazmino, S.V. Lomov, A.E. Bogdanovich, D.D. Mungalov, I. Verpoest, Quasi-static and fatigue tensile behavior of a 3D rotary braided carbon/epoxy composite, J Compos Mater 47 (2013) 3195–3209, http://dx.doi.org/10.1177/0021998312463407.

[15] Celanese – Ticona GmbH, 2016. [Online]. Available: <http://tools.ticona.com/tools/mcbasei/product-tools.php>.

[16] S.G. Ivanov, D. Beyens, L. Gorbatikh, S.V. Lomov, Damage development in woven carbon fibre thermoplastic laminates with PPS and PEEK matrices: a comparative study, J Compos Mater (2016) http://dx.doi.org/10.1177/0021998316653460.

[17] Correlated Solutions, Inc., VIC-2D, Irmo, SC, USA: <http://www.correlatedsolutions.com>, 2012.

[18] G.J. Curtis, J.M. Milne, W.N. Reynolds, Non-Hookean behaviour of strong carbon fibres, Nature 220 (1968) 1024–1025.

[19] M. Shioya, E. Hayakawa, A. Takaku, Non-hookean stress-strain response and changes in crystallite orientation of carbon fibres, J Mater Sci 31 (1996) 4521–4532.

[20] P. Parlevliet, H. Bersee, A. Beukers, Residual stresses in thermoplastic composites – a study of the literature – part I: formation of residual stresses, Composites A 37 (11) (2006) 1847–1857, http://dx.doi.org/10.1016/j.compositesa.2005.12.025.

[21] P. Parlevliet, H. Bersee, A. Beukers, Residual stresses in thermoplastic composites – a study of the literature – part III: effects of thermal residual stresses, Composites A 38 (6) (2007) 1581–1596, http://dx.doi.org/10.1016/j.compositesa.2006.12.005.

[22] S. Daggumati, W. Van Paepegem, J. Degrieck, T. Praet, B. Verhegghe, J. Xu, et al., Local strain in a 5-harness satin weave composite under static tension: part II – Meso-FE analysis, Compos Sci Technol 71 (2011) 1217–1224, http://dx.doi.org/10.1016/j.compscitech.2011.03.020.

[23] N. Godin, S. Huguet, R. Gaertner, L. Salmon, Clustering of acoustic emission signals collected during tensile tests on unidirectional glass/polyester composite using supervised and unsupervised classifiers, NDT&E Int 37 (2004) 253–264, http://dx.doi.org/10.1016/j.ndteint.2003.09.010.

[24] S. Huguet, N. Godin, R. Gaertner, L. Salmon, D. Villard, Use of acoustic emission to identify damage modes in glass fibre reinforced polyester, Compos Sci Technol 62 (2002) 1433–1444, http://dx.doi.org/10.1016/S0266-3538(02)00087-8.

[25] F. Yu, Y. Okabe, Q. Wu, N. Shigeta, A novel method of identifying damage types in carbon fiber-reinforced plastic crossply laminates based on acoustic emission detection using a fiber-optic sensor, Compos Sci Technol 135 (27) (2016) 116–122, http://dx.doi.org/10.1016/j.compscitech.2016.09.017.